Journal of Alloys and Compounds 512 (2012) 278–281

Contents lists available at SciVerse ScienceDirect

Journal of Alloys and Compounds

journal homepage: www.elsevier.com/locate/jallcom

On the stability of the Higher Manganese Silicides

Ali Allam [a], Carlos Angelo Nunes [b], Jakub Zalesak [a], Marie-Christine Record [a,*]

[a] IM2NP, UMR 6242 CNRS – Université Aix-Marseille, av Escadrille Normandie-Niemen, Case 142, 13397 Marseille Cedex 20, France
[b] Departamento de Engenharia de Materiais (DEMAR), Escola de Engenharia de Lorena (EEL), Universidade de São Paulo (USP), Caixa Postal 116, 12600-970 Lorena, São Paulo, Brazil

ARTICLE INFO

Article history:
Received 28 July 2011
Received in revised form
10 September 2011
Accepted 13 September 2011
Available online 5 October 2011

Keywords:
HMS
Phase equilibria
Phase transformations
Stability range
Manganese
Silicides

ABSTRACT

We investigated in this work the stability of the Higher Manganese Silicides (HMS). Several alloys in the composition range 62–66 at.% Si were prepared from their constitutive elements by arc-melting. The prepared alloys were then analysed by in situ X-ray diffraction measurements and Electron Probe Micro-Analyser (EPMA). The whole results allow us to suggest that whatever the composition is, only $Mn_{27}Si_{47}$ is stable for the temperatures 500 °C and 800 °C. At higher temperatures, the studied samples undergo two phase transformations which consecutively lead to the formation of $Mn_{15}Si_{26}$ and $Mn_{11}Si_{19}$. Mn_4Si_7 was never evidenced in the present work. It is shown for the first time in this work that $Mn_{27}Si_{47}$ is the only HMS stable phase at room temperature.

1. Introduction

The semiconductors Higher Manganese Silicides $MnSi_x$ ($x = 1.72–1.75$) also known as HMS are the highest silicon-rich intermediate phases in the manganese–silicon binary phase diagram. These compounds have attracted much attention in recent years because of their applications in spintronics, such as ferromagnetic semiconductors, and in thermoelectrics due to their large Seebeck coefficient, low resistivity, and high oxidation resistance [1–3]. Besides, they are non-toxic and cheap.

In previous studies, HMS has been successfully synthesized using different methods: solid phase reaction, sputtering, reactive deposition epitaxy, and chemical reaction [4–7]. However, there are some disagreements in the reported physical properties of HMS [8], and it was suggested that these discrepancies come from the subtle structural differences in the complex crystal structures of HMS [6]. Four HMS Mn_4Si_7 [9], $Mn_{11}Si_{19}$ [10], $Mn_{15}Si_{26}$ [11], and $Mn_{27}Si_{47}$ [12] are reported in literature. These phases are referred to as the "Nowotny chimney ladder" phase being derived from a $TiSi_2$ parent structure [13]. They all possess a tetragonal unit cell with high anisotropy. The 'a' lattice parameter is the same for all the structures since the 'c' one is different. These structures consist in "chimney" Si and "ladder" Mn sublattices.

To optimize physical properties of HMS for applications, knowledge on the crystal structure, the composition, and the phase stability of HMS is required. The stability range of these HMS phases has not been determined so far. The Mn–Si phase diagram reports a homogeneity range around $MnSi_{1.75}$ [14] without giving information on these different structures. Therefore the aim of this work was to investigate the stability range of the HMS phases.

We prepared several alloys in the composition range 62–66 at.% Si, from their constitutive elements by arc-melting and we studied their stability range in temperature by using X-ray diffraction measurements and Electron Probe Micro-Analyser (EPMA).

2. Experimental details

The Mn_xSi_y alloys were synthesized from their constitutive elements, Mn (99.8%) and Si (99.999%), by arc melting in a water-cooled copper crucible under argon (99.995%). Mn and Si elements were weighed in different atomic percentages. The compositions of the prepared alloys are as follows: $Mn_{38}Si_{62}$, $Mn_{37}Si_{63}$, $Mn_{36}Si_{64}$, $Mn_{35}Si_{65}$, and $Mn_{34}Si_{66}$. Three melting steps were carried out for each alloy in order to produce chemically homogeneous samples. After arc melting all the ingots were encapsulated in quartz tubes under argon, heat-treated at 500 °C and 800 °C for 2 weeks and 1 week, respectively and then quenched in water at room temperature. These annealings were performed in order to reach the equilibrium state.

The X-ray diffraction patterns were recorded on a Philips X'pert system using the Cu Kα radiation with the Bragg–Brentano geometry and an Xcelerator X-ray detector. Two different kinds of XRD analysis were carried out: analysis at room temperature, and in situ analysis. For in situ high temperature (HT) XRD measurements, the samples were loaded into an XRD chamber, equipped with a heating stage in a vacuum of about 10^{-5} mbar. The XRD measurements were performed each 20 °C from 100 to 1000 °C. The heating rate was 5 °C/min. The diffractograms were recorded in the [20–60°] 2θ range, with a step size of 0.02° and a step time of 10 s.

* Corresponding author. Tel.: +33 491282884; fax: +33 491282886.
E-mail address: m-c.record@univ-cezanne.fr (M.-C. Record).

0925-8388/$ – see front matter © 2011 Elsevier B.V. All rights reserved.
doi:10.1016/j.jallcom.2011.09.081

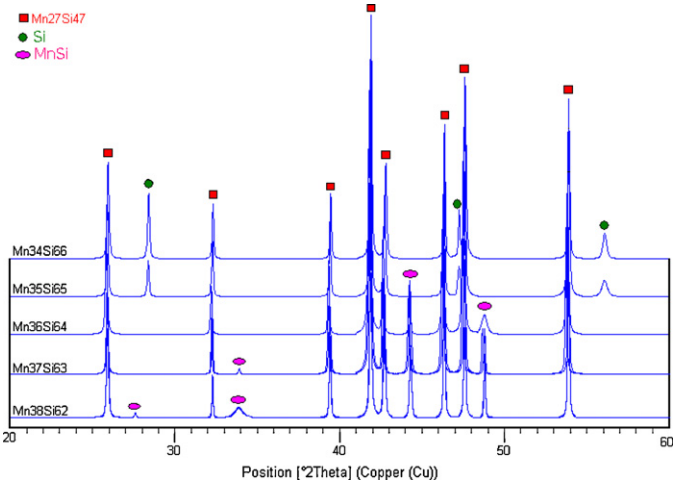

Fig. 1. XRD patterns recorded at room temperature for samples annealed at 500 °C for 2 weeks.

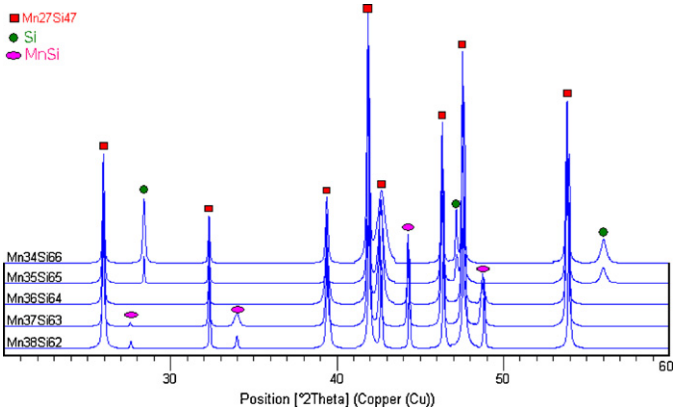

Fig. 2. XRD patterns recorded at room temperature for samples annealed at 800 °C for 1 week.

Electron Probe Micro-Analyser (EPMA, CAMECA SX100) was used in the following conditions: $U = 20$ kV and $I = 4$ nA.

3. Results and discussion

3.1. XRD diffraction at room temperature

Figs. 1 and 2 show the XRD patterns recorded at room temperature on samples annealed at 500 °C for 2 weeks, and at 800 °C for 1 week, respectively.

Table 1
Chemical compositions obtained by EPMA analysis on samples $Mn_{34}Si_{66}$ and $Mn_{38}Si_{62}$ annealed at 800 °C.

	$Mn_{34}Si_{66}$ (a)	$Mn_{38}Si_{62}$ (b)
Dark phase	97.97% Si 2.02% Mn	63.11% Si 36.88% Mn
Light phase	63.14% Si 36.85% Mn	50.35% Si 49.64% Mn

The analysis of Fig. 1 shows that the samples $Mn_{38}Si_{62}$, $Mn_{37}Si_{63}$ and $Mn_{36}Si_{64}$ contain ($MnSi + Mn_{27}Si_{47}$). We can notice that the intensity of the MnSi peaks decreases with the increase of the silicon content. For the samples $Mn_{35}Si_{65}$ and $Mn_{34}Si_{66}$, they are constituted of ($Si + Mn_{27}Si_{47}$), and the intensity of the Si peaks increases with the Si atomic percentage.

Therefore whatever the composition, the HMS present in the samples annealed at 500 °C is $Mn_{27}Si_{47}$. The same conclusion can be deduced from Fig. 2 for samples annealed at 800 °C.

Our samples can be classified into two groups of composition: one containing MnSi and $Mn_{27}Si_{47}$, the other containing $Mn_{27}Si_{47}$ and Si and $Mn_{27}Si_{47}$ is the only HMS phase present in samples annealed both at 500 and 800 °C.

3.2. EPMA analysis

We analysed by EPMA all the samples that we prepared, however since these samples can be classified into two groups of compositions, and in sake of clarity, we only present in this article the results obtained for the end member alloys $Mn_{38}Si_{62}$ and $Mn_{34}Si_{66}$ annealed at 800 °C. The results are presented in Fig. 3a and b for $Mn_{38}Si_{62}$ and $Mn_{34}Si_{66}$, respectively. Both samples are constituted of two phases. The chemical compositions of these phases are given in Table 1. In agreement with the X-ray diffraction results, $Mn_{38}Si_{62}$ contains (MnSi + HMS) and $Mn_{34}Si_{66}$ is constituted of (HMS + Si). The composition of the HMS is approximately the same in both samples (63.15 at.% Si and 36.85 at.% Mn). These results support the X-ray diffraction results; only one HMS is stable at 800 °C. Since the accuracy of the EPMA analysis is around 0.5 at.% and the reliability of X-ray diffraction measurements is high, we can suggest based on XRD results that the stable HMS is $Mn_{27}S_{47}$.

3.3. In situ XRD

As for the EPMA analysis, we investigated all the samples by using in situ X-ray diffraction measurements but we only show in this paper the results obtained for the end-member alloys ($Mn_{34}Si_{66}$ and $Mn_{38}Si_{62}$) annealed at 800 °C. The XRD patterns of $Mn_{34}Si_{66}$ and $Mn_{38}Si_{62}$ are presented in Figs. 4 and 5, respectively.

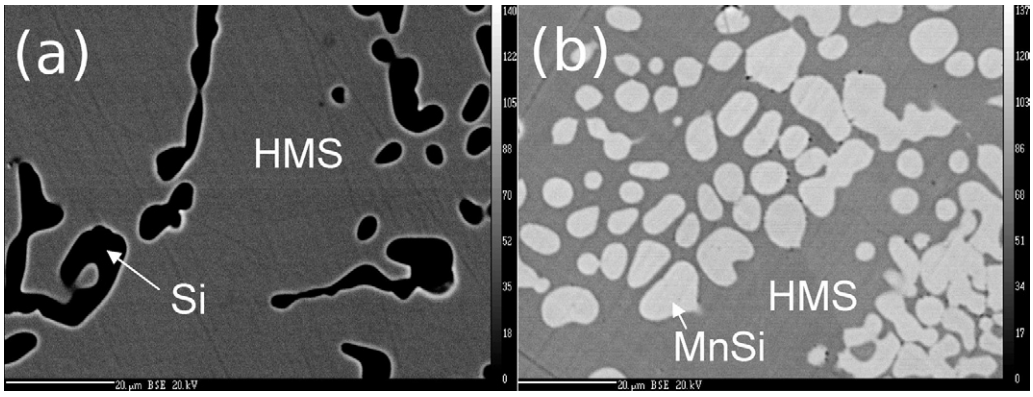

Fig. 3. EPMA micrographs of samples annealed at 800 °C (a) $Mn_{34}Si_{66}$ and (b) $Mn_{38}Si_{62}$.

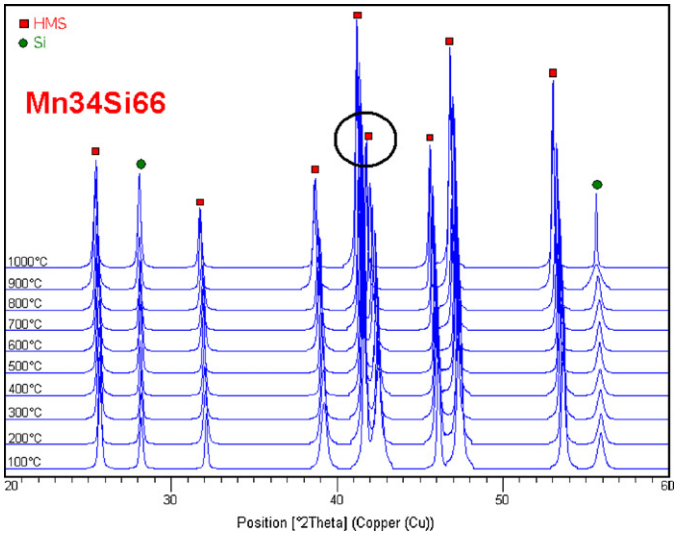

Fig. 4. In situ XRD diffractograms $Mn_{34}Si_{66}$ annealed at 800 °C.

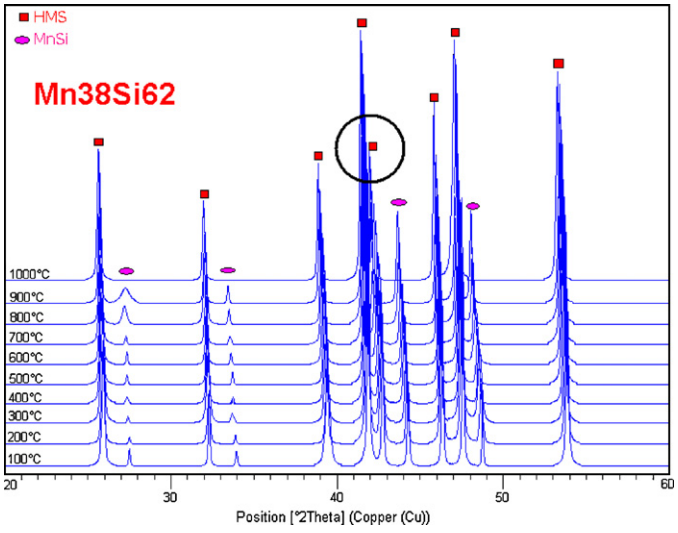

Fig. 5. In situ XRD patterns of $Mn_{38}Si_{62}$ annealed at 800 °C.

One can observe for both samples that all the diffraction peaks are shifted towards the lower angles when the temperature increases. However, this shift is much bigger in the case of the peak at $2\theta = 43°$. Moreover the intensities corresponding to the peaks of MnSi or Si change during the heating. These evolutions from 25 °C to 1000 °C are presented in Fig. 6. For the $Mn_{38}Si_{62}$ sample, the quantity of MnSi is stable from room temperature up to 820 °C, then it increases up to 880 °C and decreases again to become null at 1000 °C. For the

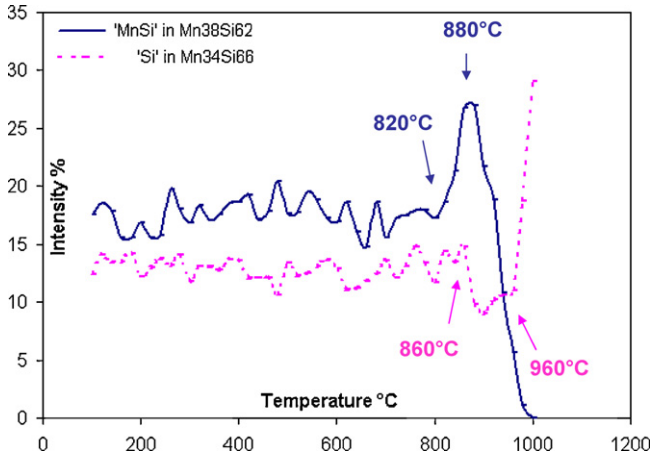

Fig. 6. Evolution of the intensity of the main peak corresponding to MnSi and Si versus temperature.

$Mn_{34}Si_{66}$ sample, the quantity of silicon is stable from room temperature to 860 °C, then it decreases and starts again to increase at 960 °C. Therefore the existence of two phase transformations during the heating is obvious for each sample. The temperatures mentioned above correspond to the starting temperatures of these transformations.

The main diffraction peaks reported for each of the HMS structures in the Pearson crystal data [15] from $2\theta = 20°$ to $2\theta = 60°$ are listed in Table 2. When comparing the diffraction peaks within the HMS series, one can notice that except for the fifth peak, it is difficult to distinguish the HMS structures from these XRD data. The intensity of the peaks does not allow us either. These observations can explain why the real structure of HMS is rarely given in literature. Usually the authors name these silicides as HMS [16], MnSi1.7 [17], or MnSi1.73 [18].

Since the most important shift is observed in our samples for the peak located at $2\theta = 43°$, we can assume that the phases which appear at high temperature correspond to HMS structures. In order to undoubtedly identify these phases, we analysed the diffraction patterns by considering the angular difference Ω between the angle corresponding to the peak number 5 and that corresponding to the peak number 4. These values calculated for all the HMS structures taking into account the Pearson's crystal data are given in Table 2. These Ω values increase as the silicon content in the HMS phase increase.

The Ω values calculated from our XRD results at the temperatures corresponding to the phase transformations are given in Table 3. A comparison with the Ω values reported in Table 2 allow us to suggest that the first phase transformation leads to the formation of $Mn_{15}Si_{26}$ whereas the second one leads to the formation of $Mn_{11}Si_{19}$. These suggestions are in agreement with the

Table 2
List of the main diffraction peaks for the four HMS phases from the Pearson's crystal data [15].

	Mn_4Si_7	$Mn_{11}Si_{19}$	$Mn_{15}Si_{26}$	$Mn_{27}Si_{47}$
Data sheet reference	550026	1301107	1251140	1251132
Lattice parameters (nm)	$a = 0.5524$	$a = 0.5518$	$a = 0.5525$	$a = 0.5523$
	$c = 1.7457$	$c = 4.8136$	$c = 6.555$	$c = 11.79$
$2\theta_1$ (°)–I (%)	26.0–37.5	25.96–41.5	25.98–39.1	25.98–37.2
$2\theta_2$ (°)–I (%)	32.38–14.4	32.42–12.8	32.38–14.8	32.36–14.8
$2\theta_3$ (°)–I (%)	39.6–30.5	39.44–29.1	39.44–29.5	39.48–30.7
$2\theta_4$ (°)–I (%)	42.0–100	42.0–100	41.98–100	41.94–100
$2\theta_5$ (°)–I (%)	43.0–28.6	42.52–30.8	42.64–29	42.8–28.5
$2\theta_6$ (°)–I (%)	46.46–35.7	46.52–38.3	46.44–37.1	46.4–34.9
$2\theta_7$ (°)–I (%)	47.7–53.1	47.62–52	47.64–54	47.66–50.9
$2\theta_8$ (°)–I (%)	54–45.9	54.04–45.3	53.98–47.5	53.94–44.7
Ω (°) $= 2\theta_5 - 2\theta_4$	1	0.52	0.66	0.86

Table 3
Ω values calculated from the experimental XRD results.

Sample	$Mn_{38}Si_{62}$		$Mn_{34}Si_{66}$	
Temperature (°C)	820	880	860	960
Ω (°)	0.6	0.55	0.64	0.6
Suggested HMS	$Mn_{15}Si_{26}$	$Mn_{11}Si_{19}$	$Mn_{15}Si_{26}$	$Mn_{11}Si_{19}$

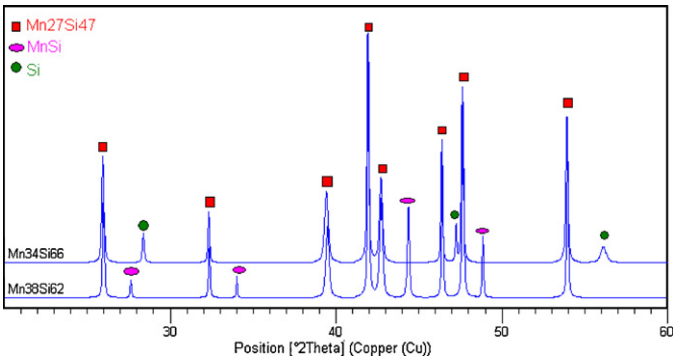

Fig. 7. XRD patterns recorded on $Mn_{38}Si_{62}$ and $Mn_{34}Si_{66}$ samples at room temperature after in situ XRD analysis.

results reported by Kawasumi et al. [3]. These authors evidenced the $Mn_{15}Si_{26}$ phase at 1100 °C in Mn–Si samples with different compositions ($MnSi_{1.7}$, $MnSi_{1.72}$, $MnSi_{1.75}$).

The high temperature phases were still present in the samples after they were cooled down. Therefore in order to check the stability of these phases, X-ray diffraction measurements were performed on these samples after keeping them at room temperature for 1 or 2 days. The XRD patterns are presented in Fig. 7. The $Mn_{38}Si_{62}$ and $Mn_{34}Si_{66}$ samples are constituted of ($Mn_{27}Si_{47}$ + MnSi) and ($Mn_{27}Si_{47}$ + Si), respectively. Thus $Mn_{27}Si_{47}$ is the only HMS phase which exists at room temperature and it is stable from room temperature up to at least 800 °C.

4. Conclusion

This work reports for the first time a detailed investigation on the stability range of the HMS phases. The stability range of these phases was studied both in temperature and in composition. Several samples with different compositions were prepared and these samples were characterized from room temperature up to 1000 °C.

The results can be summarized as follows:

- $Mn_{27}Si_{47}$ is the only HMS phase stable at room temperature.
- $Mn_{27}Si_{47}$ is stable from room temperature to at least 800 °C.
- Two phase transformations were found at high temperatures in the studied samples.
- $Mn_{15}Si_{26}$ and $Mn_{11}Si_{19}$ were evidenced in samples with silicon content lower than 64 at.% for temperatures higher than 820 °C and 880 °C, respectively.
- $Mn_{15}Si_{26}$ and $Mn_{11}Si_{19}$ were evidenced in samples with silicon content higher than 64 at.% for temperatures higher than 860 °C and 960 °C, respectively.

References

[1] M.C. Bost, J.E. Mahan, J. Electron. Mater. 16 (1987) 389.
[2] S. Zhou, K. Potzger, G. Zhang, A. Mücklich, F. Eichhorn, N. Schell, R. Grötzschel, B. Schmidt, W. Skorupa, M. Helm, J. Fassbender, D. Geiger, Phys. Rev. B 75 (2007) 085203.
[3] I. Kawasumi, M. Sakata, I. Nishida, K. Masumoto, J. Mater. Sci. 16 (1981) 355.
[4] M. Eizenberg, K.N. Tu, J. Appl. Phys. 53 (1982) 6885.
[5] S. Teichert, H. Hortenbach, H.-J. Hinneberg, Appl. Phys. Lett. 78 (2001) 1988.
[6] S. Teichert, R. Kilper, J. Erben, D. Franke, B. Gebhard, Th. Franke, P. Häussler, W. Henrion, H. Lange, Appl. Surf. Sci. 104–105 (1996) 679.
[7] J.M. Higgins, A.L. Schmitt, I.A. Guzei, S. Jin, J. Am. Chem. Soc. 130 (2008) 16086.
[8] J.E. Mahan, Thin Solid Films 461 (2004) 152.
[9] O.G. Karpinskii, B.A. Evseev, Izv. Akad. Nauk SSSR, Neorg. Mater. 5 (1969) 525.
[10] O. Shwomma, A. Preisinger, H. Nowotny, A. Wittman, Monatsh. Chem. 95 (1964) 1527.
[11] H.W. Knott, M.H. Mueller, L. Heaton, Acta Crystallogr. 23 (1967) 549.
[12] G. Zwilling, H. Nowotny, Monatsh. Chem. 102 (1971) 672.
[13] H. Nowotny, in: L. Eyring, M. O'Keefe (Eds.), The Chemistry of Extended Defects in Non-metallic Solids, North-Holland, Amsterdam, 1970, p. 223.
[14] T.B. Massalski, Binary Alloys Phase Diagrams, ASM, Materials Park, OH, 1996.
[15] P. Villars, K. Cenzual, Pearson's Crystal Data – Crystal Structure Database for Inorganic Compounds, Release 2010/11, ASM International, Materials Park, OH, USA, 2011.
[16] A.J. Zhou, X.B. Zhao, T.J. Zhu, S.H. Yang, T. Dasgupta, C. Stiewe, R. Hassdorf, E. Mueller, Mater. Chem. Phys. 124 (2010) 1001.
[17] J. Hu, C. Zhang, W. Li, S. Guan, H. Tatsuoka, Phys. Proc. 11 (2011) 138.
[18] T. Itoh, M. Yamada, J. Electron. Mater. 38 (7) (2009) 925.